Liquid Gallium Nanospheres Emitting White Light

*Jin Xiang, Jingdong Chen, Shuai Jiang, Mingcheng Panmai, Peilian Li, Yi Xu, Qiaofeng Dai, Shaolong Tie, and Sheng Lan**

Gallium (Ga) is not only a metal possessing surface plasmon resonance in the ultraviolet region but also a phase-change material with very low melting point. Spherical Ga nanoparticles composed of liquid Ga cores and solid Ga_2O_3 shells, which exhibit surface plasmonic resonances spanning the ultraviolet to near-infrared spectral region, are fabricated by using femtosecond laser ablation. Under the excitation of femtosecond laser light, only second harmonic generation is observed in the Ga nanospheres placed on a glass substrate. In sharp contrast, white light emission can be generated in such Ga nanospheres when they are placed on a thin silver film. It is revealed numerically and confirmed experimentally that a Fano resonance originating from the interference between the mirror-image-induced magnetic dipole mode and the gap plasmon mode is formed in the backward scattering spectra of the Ga nanospheres. Efficient white light emission can be achieved by resonantly exciting either the magnetic dipole resonance or the Fano resonance. Based on spectral analysis, the white light emission is identified as the hot-electron intraband luminescence. The fabricated core–shell Ga nanospheres provide an ideal platform on which the optical properties and practical applications of liquid Ga nanoparticles can be systematically investigated.

1. Introduction

Gallium (Ga) nanoparticles have attracted great interest in recent years because Ga is not only a metal possessing surface plasmon resonance in the ultraviolet region[1–7] but also a phase-change material with a very low melting temperature (29.7 °C).[8,9] The potential applications of the ultraviolet plasmonic resonances of Ga nanoparticles include optical memory,[10] environmental remediation, and simultaneous fluorescence and surface-enhanced Raman spectroscopies.[3,4] As compared with other metals which exhibit plasmonic resonances in the ultraviolet region,[5,11–19] such as silver (Ag)[14] and aluminum,[15–19] Ga nanoparticles remain to be quite stable in atmosphere because of the existence of a thin native gallium trioxide (Ga_2O_3) shell.[20] Another intriguing characteristic of Ga nanoparticles is the so-called supercooling phenomenon.[21–23] It means that liquid Ga nanoparticles are transformed into solid ones at a temperature much lower than the melting point of bulk Ga. In addition, the phase transition temperature depends strongly on the sizes of Ga nanoparticles.[23] This unique feature of Ga nanoparticles offers us the opportunity to study the linear and nonlinear optical properties of Ga nanoparticles in liquid phase at room temperature, which possess a Drude-like dielectric function extending from the ultraviolet to near-infrared spectral region.[2] So far, the studies on the optical and plasmonic properties of Ga nanoparticles are limited to the linear optics regime. The nonlinear optical properties of Ga nanoparticles under the excitation of femtosecond laser pulses remain unexplored.

So far, Ga nanoparticles have been generally fabricated by using bottom-up techniques, such as self-assembly during molecular beam epitaxy,[1–4] optically regulated self-assembly, thermal evaporation,[24–26] and colloidal synthesis.[23,27] However, the dense irregular Ga nanoparticles obtained by using molecular beam epitaxy make optical characterization of individual Ga nanoparticles quite difficult. In addition, several factors, such as contact angle, substrate material, and surface oxidation, needed to be considered in order to accurately describe the scattering properties of such irregular Ga nanoparticles. Spherical Ga nanoparticles or Ga nanospheres (NSs) are obtained only by using chemical methods (such as colloidal synthesis) and their

J. Xiang, Dr. J. Chen, S. Jiang, M. Panmai, Dr. Q. Dai, Prof. S. Lan
Guangdong Provincial Key Laboratory of Nanophotonic Functional Materials and Devices
School of Information and Optoelectronic Science and Engineering
South China Normal University
Guangzhou 510006, China
E-mail: slan@scnu.edu.cn

P. Li
Institute for Advanced Materials and Guangdong Provincial Key Laboratory of Quantum Engineering and Quantum Materials
South China Academy of Advanced Optoelectronics
South China Normal University
Guangzhou 510006, China

Dr. Y. Xu
Department of Electronic Engineering
College of Information Science and Technology
Jinan University
Guangzhou 510632, China

Prof. S. Tie
School of Chemistry and Environment
South China Normal University
Guangzhou 510006, China

The ORCID identification number(s) for the author(s) of this article can be found under https://doi.org/10.1002/lpor.201800214

DOI: 10.1002/lpor.201800214

diameters are limited to be smaller than 100 nm.[23] In this case, the electric dipole (ED) resonances of such Ga NSs appear in the ultraviolet spectral region, making it difficult to characterize their optical properties. Spherical Ga particles with diameters of a few micrometers can be obtained by using top-down methods, such as channelless fabrication and ultrasonic treatment.[27] However, such Ga microparticles are not suitable for studying the optical properties in the visible to near-infrared spectral region. Therefore, the achievement of Ga NSs which exhibit surface plasmon resonances in the visible to near-infrared spectral region by using a top-down technique remains a big challenge.

Recently, it has been demonstrated that femtosecond laser ablation can be employed to fabricate semiconductor nanoparticles, such as silicon (Si) NSs which exhibit distinct electric and magnetic resonances in the visible to near-infrared spectral region.[28–32] Based on Mie theory and the complex refractive index reported for liquid Ga,[33] one can expect that the ED and electric quadrupole (EQ) resonances of a liquid Ga NS will be shifted from the ultraviolet to visible light and even near-infrared spectral region with increasing diameter of the liquid Ga NS (see Figure S1, Supporting Information). Therefore, it is quite interesting to study the coherent interaction between the ED and EQ of a liquid Ga NS, which may lead to highly directional radiation based on the generalized Kerker's condition.[34] More importantly, the redshift of the ED resonance to the visible light and near-infrared spectral region offers us the opportunity to explore the nonlinear optical responses of liquid Ga NSs under the excitation of femtosecond laser pulses. The disordered arrangement of Ga atoms in liquid phase (i.e., non-periodic arrangement) provides an environment with significantly reduced carrier-phonon coupling which may facilitate the radiative recombination of hot carriers.

Efficient broadband nanoscale emitters operating at optical frequencies have attracted great interest in recent years because they are highly desirable in many applications, such as ultracompact optical chips, bioimaging, nanospectroscopy, and active photonic devices. However, the achievement of efficient nanoscale white-light source remains a major fundamental challenge.[35,36] Very recently, efficient white light emission, which is known as hot-electron luminescence, has been achieved in Si and GaAs nanoparticles by resonantly exciting their Mie resonances, especially the magnetic dipole (MD) resonances.[30,31] The physical origin is the strongly localized electric field at the MD resonance of a nanoparticle, leading to a significantly enhanced multiphoton-induced absorption which is proportional to the integration of $|E|^n$ over the volume of the nanoparticle. If the excitation wavelength is far from the resonances, the nonlinear response spectra of Si/GaAs nanoparticles are dominated by second harmonic generation (SHG) rather than hot-electron luminescence. For metallic nanoparticles with diameters larger than 100 nm, such as Au/Ag NSs and Ga NSs studied in this work, there are only broad ED resonances with very low quality factors owing to the large ohmic loss in the visible light spectrum (see Figure S1, Supporting Information). In addition, the electric field is mainly localized outside the nanoparticle and the multiphoton-induced absorption is quite small at the electric resonances.[37,38] Different from small metallic nanoparticles, the extinction of such large metallic nanoparticles is dominated by scattering rather than absorption. Therefore, the hot-electron luminescence is generally very weak even though large metallic nanoparticles are resonantly excited at their ED resonances. However, the situation can be dramatically changed by bringing them to the surface of a thin metal film. It is known that a mirror image of the ED of a metallic nanoparticle can be induced by the thin metal film and the coherent interaction between the ED and its mirror image leads to the formation of a MD resonance with a narrower linewidth.[39] Consequently, efficient photoluminescence is anticipated when the metallic nanoparticle is excited resonantly at the MD resonance by using femtosecond laser pulses. In some cases, Fano resonance, which is formed by the coherent interaction of a bright mode with a broad linewidth and a dark mode with a narrow linewidth,[40,41] can be created, leading to a significantly enhanced electric field which is quite useful for nonlinearity enhancement.[42] More efficient photoluminescence can be expected by exploiting the resonant excitation of the Fano resonance, as demonstrated in this work.

Herein, we show that Ga NSs composed of liquid Ga cores and Ga_2O_3 shells can be fabricated by using femtosecond laser ablation and the surface plasmon resonances of such Ga NSs can be tuned in the visible to near-infrared spectral region by simply varying the diameter of Ga NSs. We investigate the nonlinear optical responses of the Ga NSs placed on a glass slide and a thin Ag film. It is found that the Ga NSs placed on the glass slide generate only second harmonic under the excitation of femtosecond laser pulses. In sharp contrast, the nonlinear response spectra of the Ga NSs placed on the thin Ag film are dominated by broadband white light emission when they are excited resonantly at the MD and Fano resonances. Based on the spectral analysis of the slope extracted from the dependence of the luminescence intensity on the excitation irradiance, the white light emission from the Ga NSs is identified as hot-electron intraband luminescence. It is revealed that the significantly enhanced electric field achieved at the mirror-image-induced MD and Fano resonances plays a crucial role in the generation of the hot electron luminescence, which possesses a lifetime shorter than 10 ps.

2. Experimental Section

2.1. Fabrication and Characterization of Ga NSs

Ga NSs with diameters ranging from 50 to 300 nm were fabricated by using femtosecond laser ablation of a Ga film immersed in water (see Figure S2, Supporting Information). A femtosecond laser amplifier (Legend, Coherent) with pulse duration of 100 fs and repetition rate of 1 kHz was employed in the ablation process. A 25-cm focal length objective was used to focus the femtosecond laser beam on the Ga film with a spot diameter of ≈40 μ m. Ga NSs ejected from the Ga film after the irradiation of femtosecond laser light were uniformly dispersed in water. Once the ablation was completed, the aqueous solution containing Ga NSs was centrifuged with a speed of 8000 rpm to separate Ga NSs with diameters of 50–300 nm from other particles. For morphology and crystallographic structure characterization, Ga NSs were dispersed on an ITO substrate (for SEM measurements) and a copper grid (for TEM measurements). For optical characterization, they were distributed on a glass slide and a thin Ag film.

The backward scattering spectra of Ga NSs were measured by using a dark-field microscope (Observer A1, Zeiss) with an

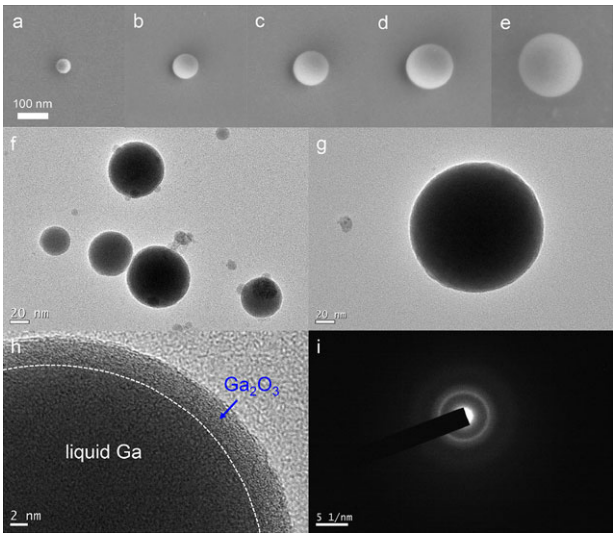

Figure 1. Morphology and structure characterization of Ga NSs. a–e) SEM images of core-shell Ga NSs with different diameters fabricated by using femtosecond laser ablation. f) TEM image of Ga NSs with different diameters. g) TEM image of a typical Ga NS with core-shell structure. h) Magnified TEM image of the Ga NS shown in (g). i) Electron diffraction pattern of a typical Ga NS.

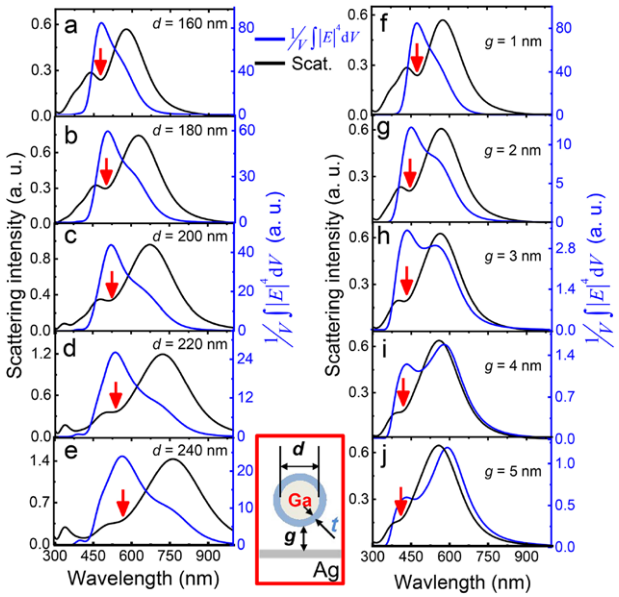

Figure 2. Fano resonance formed in the scattering spectra of Ga NSs placed on the Ag film. a) Backward scattering spectra calculated for Ga NSs with a fixed gap width of $g = 0$ nm and different diameters. b) Backward scattering spectra calculated for the Ga NS with $d = 160$ nm and different gap widths. In each case, the spectrum of $[\int |E(\lambda)|^4 dV]/V$ for the Ga NS is also provided.

external white light source for illumination. The incident light can be either *s*- or *p*-polarized by using a polarizer. The characterization of the nonlinear optical properties of Ga NSs were carried out by using a femtosecond laser oscillator (Mira-HP, Coherent) and an optical parametric oscillator (Mira OPO-X, Coherent) with pulse duration of 130 fs and repetition rate of 76 MHz (see Figure S3, Supporting Information). The femtosecond laser light was introduced into an inverted microscope and focused on Ga NSs by using a 100× objective. The nonlinear optical signals from Ga NSs were collected by the same objective and directed to a spectrometer (SR500, Andor) for analysis.

2.2. Numerical Simulation and Analytical Model

The scattering spectra of Ga NSs placed on a glass slide or a thin Ag film were calculated by using Mie theory or simulated by using the finite-difference time domain (FDTD) technique (commercial software developed by Lumerical Solution Inc. (http://www.lumerical.com). In the FDTD simulation, the smallest non-uniform mesh size of 1 nm, as well as a perfectly matched boundary condition, was employed. The complex refractive index of Ag is from ref. [43]. The complex refractive indices for liquid cores of Ga and solid shells of Ga_2O_3 used in the numerical simulations are provided in Figure S4, Supporting Information.

3. Results and Discussion

Ga NSs with diameters (d) ranging from 50 to 300 nm were fabricated by using femtosecond laser ablation (see Figure S2, Supporting Information for details). In **Figure 1**a–e, we show the scanning electron microscopy (SEM) images of typical Ga NSs with different diameters. It can be seen that the fabricated Ga NSs possess spherical shape and smooth surface. A clear core-shell structure can be identified in Figure 1f–h in which the transmission electron microscopy (TEM) images of a few Ga NSs and a single Ga NS, respectively, are provided. The thickness of the Ga_2O_3 shell was estimated to be $t \approx 2.0$ nm (see Figure 1h). The electron diffraction pattern of a typical Ga NS, which clearly indicates the liquid core of the Ga NS, is shown in Figure 1i.

3.1. Fano Resonances Formed in the Scattering Spectra of Ga NSs Placed on a Thin Ag Film

We first examined the scattering properties of Ga NSs with core-shell structures placed on a 50-nm-thick Ag film. In **Figure 2**a–e, we present the backward scattering spectra simulated for Ga NSs with different diameters ranging from 160 to 240 nm. In all cases, the thickness of the Ga_2O_3 shell and the gap width between the Ga NS and the Ag film were chosen to be $t = 2.0$ nm and $g = 0$ nm, respectively. For the Ga NS with $d = 160$ nm, one can see two scattering peaks separated by a scattering valley. With increasing diameter of the Ga NS, a rapid increase of the scattering intensity, as well as a large redshift of the resonant wavelength, is observed for the main scattering peak at the longer wavelength. In comparison, only a small redshift is found for the weak scattering peak and its intensity remains nearly unchanged. As a result, it degenerates eventually as a small shoulder of the main scattering peak at $d = 240$ nm. In addition, it is noticed that the scattering valley is also redshifted with increasing diameter of the Ga NS and it becomes not so obvious in the scattering spectrum

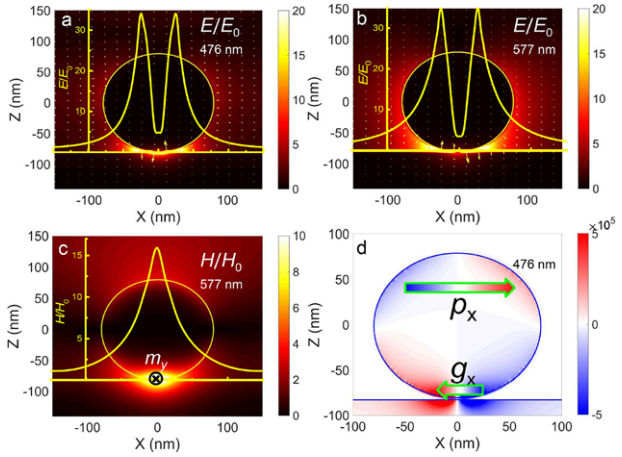

Figure 3. Electric and magnetic field enhancements at the mirror-image-induced MD and the Fano dip. The electric field distributions calculated for the Ga NS with $d = 160$ nm at a) the Fano dip and b) the mirror-image-induced MD resonance. c) Magnetic field distribution calculated at the MD resonance. d) Electric current distribution calculated for the Ga NS at the Fano dip. In (a)–(c), a 1D electric or magnetic field distribution along the *x* axis is also is provided.

of the Ga NS with $d = 240$ nm. Under the normal incidence of a plane wave propagating in the *z*-direction, an ED mode and a gap plasmon (GP) mode oriented both in the *x*-direction (i.e., p_x and g_x) will be excited in the Ga NS (see **Figure 3** for the coordinate). Owing to the existence of the Ag film, an anti-parallel ED, which is the mirror image of the original ED, will be induced.[44–46] The coherent interaction of these two anti-parallel EDs leads to the formation of a MD mode oriented in the *y*-direction (m_y). Consequently, the scattering of the Ga NS in the far field is determined by the coherent interaction between the mirror-image-induced MD mode (m_y) and the GP mode (g_x). Basically, the resonant wavelength of the MD mode depends on the distance between the two anti-parallel EDs, which is approximately equal to the diameter of the Ga NS. Therefore, it is expected that the resonant wavelength of the MD mode is redshifted with increasing diameter of the Ga NS. In comparison, the resonant wavelength of the GP mode is not so sensitive to the diameter of the Ga NS. Thus, a slight redshift of the resonant wavelength is anticipated for the GP mode. Based on the above analysis, the main scattering peak observed in the scattering spectrum of the Ga NS is attributed to the mirror-image-induced MD mode while the scattering valley is actually the Fano resonance (or Fano dip) originating from the destructive interference between the MD mode with a broad band and the GP mode with a narrow band. In order to confirm this assignment, we calculated the spectra of $[\int |E(\lambda)|^4 \mathrm{d}V]/V$ (V is the volume of the Ga NS), which represents two-photon-induced absorption (TPA),[30,47,48] for Ga NSs with different diameters, as shown in Figure 2a–e. In all cases, it can be seen that the maximum of $[\int |E(\lambda)|^4 \mathrm{d}V]/V$ appears at the scattering valley. Since the Fano resonance is generally accompanied by a significantly enhanced electric field, the coincidence of the maximum of $[\int |E(\lambda)|^4 \mathrm{d}V]/V$ with the scattering valley undoubtedly confirms that the scattering valley is actually a Fano dip.

In order to create an obvious Fano dip, the bright and dark modes interacting coherently are requested to be anti-phase. In addition, their amplitudes should be comparable. In our case, the amplitude of the GP mode is quite sensitive to the gap width while that of the MD mode is not. As a result, it is expected that the Fano dip observed in the case of a small gap width will disappear for a large gap width. In Figure 2f–j, we present the evolution of the backward scattering spectrum of the Ga NS with $d = 160$ nm with increasing gap width. As expected, the Fano dip becomes less pronounced when the gap width is increased to $g = 5$ nm. In addition, a small blueshift of the Fano dip is observed. It is noticed that the resonant wavelength of the main scattering peak remains nearly unchanged when the gap width is changed. This feature further verifies that the main scattering peak originates from the coherent interaction of the ED and its mirror image because the resulting MD resonance is determined mainly by the diameter of the GS NS and is not sensitive to the small variation of the gap width.

3.2. Field Enhancements at the Magnetic Dipole and Fano Resonances

In order to gain a deep insight into the significantly enhanced electric field achieved at the Fano dip, we calculated the electric field distribution at the Fano dip (≈476 nm) for a Ga NS with $d = 160$ nm, as shown in Figure 3a. It can be seen that the electric field is concentrated at the gap region which is a characteristic of the GP mode. For comparison, we also calculated the electric and magnetic field distributions at the mirror-image-induced MD resonance (≈577 nm), as shown in Figure 3b,c. In this case, the strong localization of the electric field at the gap region is also observed. Different from the electric field distribution observed at the Fano dip, an enhancement in the electric field on both sides of the Ga NS is observed, corresponding to the ED (p_x) induced in the Ga NS. If we examine the magnetic field distribution, it is found that the maximum of the magnetic field is located at the center of the gap region with its orientation in the *y*-direction, as shown in Figure 3c. It verifies the formation of a mirror-image-induced MD at the gap center. In Figure 3d, we present the electric current distribution calculated at the Fano dip which indicates clearly the phases of the ED and GP modes (p_x and g_x). It can be seen that the ED and GP modes are out of phase, implying that the MD and GP modes are also out of phase because the ED and MD modes are in phase (see Figure 3c). Therefore, it confirms that the Fano dip created in the backward scattering spectrum really originates indeed from the destructive interference of the MD and GP modes.

3.3. Revealing Fano Resonances in the Scattering Spectra of Ga NSs

As discussed above, the Fano dip originating from the destructive interference between the mirror-image-induced MD mode and the GP mode generally appears as a scattering valley in the backward scattering spectrum of a Ga NS. In Figure 2, we have investigated the evolution of the backward scattering spectrum of a Ga NS placed on the Ag film with increasing diameter and gap width. For simplicity, the Ga NS is illuminated by a normally incident plane wave. In practice, however, one can only measure

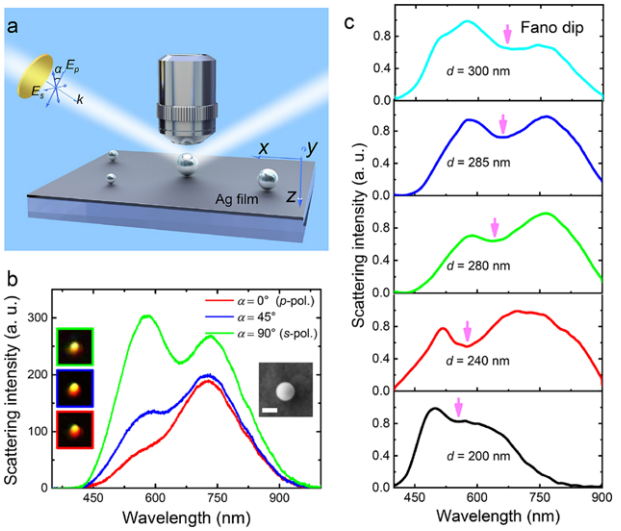

Figure 4. Revealing the Fano resonances in the backward scattering spectra of Ga NSs. a) Schematic showing the characterization of the scattering properties of Ga NSs placed on a thin Ag film by using polarized white light. b) Backward scattering spectra measured for a Ga NS with $d \approx 320$ nm by using white light with different polarization angles of 0° (*s*-polarized), 45°, and 90° (*p*-polarized). The SEM image of the Ga NS and the radiation patterns recorded by using a charge-coupled device are shown in the insets. c) Backward scattering spectra measured for Ga NSs with different diameters placed on the Ag film.

the backward scattering spectrum of a Ga NS illuminated by an obliquely incident plane wave. In this case, the incident light can be either *s*- or *p*-polarized, as schematically shown in **Figure 4**a. For *s*-polarized light, only the horizontally oriented ED (p_x) and GP modes (g_x) will be excited, leading to the formation of mirror-image-induced MD (m_y) and the Fano dip. The situation is more complicated for *p*-polarized light because both horizontally (p_x and g_x) and vertically (p_z and g_z) oriented ED and GP modes can be excited. Since the MD induced by p_z and its mirror image appears in the near-infrared spectral region,[39,49] the Fano dip still arises from the destructive interference between m_y and g_x, similar to that observed for *s*-polarized light. We have simulated the backward scattering spectra for a Ga NS with $d \approx 240$ nm illuminated by *s*- and *p*-polarized light and calculated the spectra of $[\int |E(\lambda)|^4 \mathrm{d}V]/V$ (see Figure S5, Supporting Information). It can be seen that the spectral shapes obtained for obliquely incident light are quite similar to those obtained for normally incident light. In addition, the maximum of $[\int |E(\lambda)|^4 \mathrm{d}V]/V$ also appears at the scattering valley, verifying that the scattering valley is actually a Fano dip. In experiments, we measured the backward scattering spectra of a Ga NS with $d \approx 240$ nm under the illumination of *s*- and *p*-polarized light, as shown in Figure 4b. In both cases, the Fano dip is clearly identified at the scattering valley. This feature can be used as a simple tool to reveal the Fano resonance formed in this particle-film hybrid system. In Figure 4c, we show the backward scattering spectra measured for Ga NSs with different diameters from which the Fano dips can be easily identified, as marked by arrows. With increasing diameter of the Ga NS, a red shift of the Fano dip is observed, in good agreement with the numerical simulation results (see Figure 2a–e).

3.4. Nonlinear Optical Responses of Ga NSs and White Light Emission

The nonlinear optical responses of Ga NSs under the excitation of femtosecond laser pulses were examined by using an inverted microscope equipped with a spectrometer (see Section 2 for details), as schematically shown in **Figure 5**a. In Figure 5b, we show the nonlinear response spectra measured for a Ga NS ($d \approx 240$ nm) sitting on a glass slide. The Ga NS was excited by using femtosecond laser light at 785 nm which coincides with the scattering peak of the Ga NS (see Figure S6, Supporting Information). In this case, we observed SHG at ≈392 nm and weak down-converted luminescence in the Stokes region. No up-converted luminescence was observed in the nonlinear response spectra. With increasing excitation irradiance, a quadratic increase of the SHG intensity was found, as shown in the inset. The Ga NSs studied in this work possess liquid Ga cores and Ga_2O_3 shells. In liquid phase, the long-range ordering of Ga atoms is lost, similar to that in amorphous materials. As a result, the SHG of liquid Ga is expected to be very weak, similar to the weak SHG observed in the liquid phase of semiconductors (Si and GaAs).[50,51] In Figure 5b, efficient SHG was observed in a Ga NS placed on a glass substrate where there are no plasmonic hot spots. Since the liquid Ga core is expected to give weak SHG, the efficient SHG might come from the Ga_2O_3 shell which is a transparent semiconductor in the visible light spectrum, similar to the efficient SHG commonly observed in ZnO and TiO_2 nanoparticles or nanostructures.[52,53]

For Ga NSs placed on the thin Ag film, the nonlinear optical responses of Ga NSs were found to be modified significantly. A typical example is shown in Figure 5c (upper part) where the nonlinear response spectra of a Ga NS ($d \approx 240$ nm) measured at different excitation irradiances are presented. In this case, the wavelength of the femtosecond laser light was chosen at the main scattering peak of the Ga NS (≈785 nm), corresponding to the mirror-image-induced MD resonance (see Figure 5d). It is noticed that the nonlinear response spectrum of the Ga was dominated by a broadband luminescence containing not only the down-converted part but also the up-converted one. In addition, the SHG almost disappears. In the lower part of Figure 5c, we present the relationship between the slope extracted from the dependence of the luminescence intensity on the excitation irradiance and the energy of the emitted photon. It is noticed that the slope is linearly proportional to the energy of the emitted photon. However, the linear relationships between the slope and the energy of the emitted photon in the low and high excitation irradiance regimes were found to be different. In the low excitation irradiance regime, the straight line has a small slope. In comparison, the slope of the straight line is increased in the high excitation irradiance regime. More interestingly, the straight line can be extrapolated to the origin of the coordinate (see Figure S7, Supporting Information). This is the unique feature of hot-electron intraband luminescence observed previously in plasmonic hot spots and semiconductor NSs.[30,54,55] This result indicates clearly that the broadband luminescence observed for the Ga NSs placed on the thin Ag film in the high excitation irradiance regime belongs to hot-electron intraband luminescence, similar to blackbody radiation.[54,55] The emission patterns of the Ga NS recorded

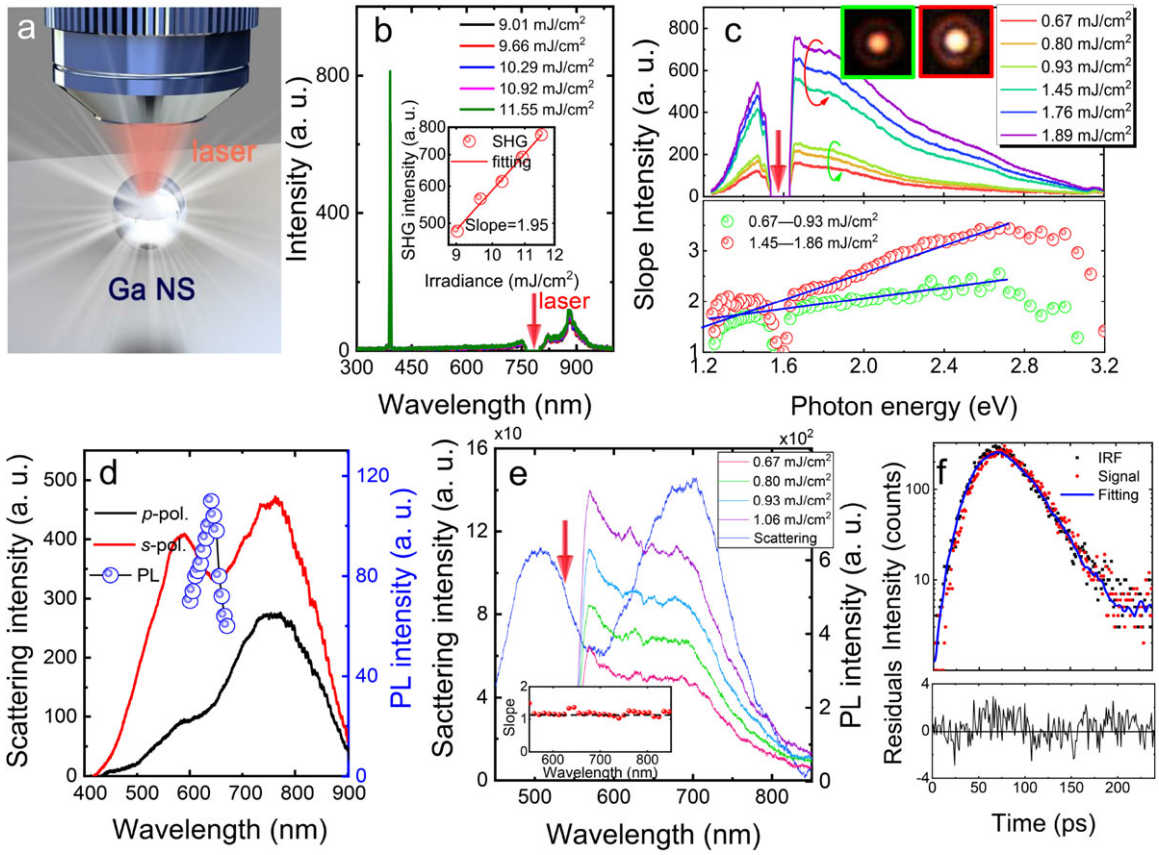

Figure 5. White light emission from Ga NSs. a) Schematic showing the excitation and detection of the nonlinear optical signals of a Ga NS. b) Nonlinear response spectra measured for a Ga NS with $d \approx 280$ nm placed on a glass slide at different excitation irradiances. The dependence of the SHG intensity on the excitation irradiance is presented in the inset. c) Nonlinear response spectra measured for a Ga NS with $d \approx 300$ nm placed on a thin Ag film at different excitation irradiances (upper part). The excitation wavelength was chosen at the MD resonance (≈785 nm). The relationship between the slope extracted from the dependence of the luminescence intensity on the excitation irradiance and the energy of the emitted photon is presented in the lower part. The emission patterns of the Ga NS recorded by using a charge-coupled device are shown in the insets. d) Excitation spectra measured for the Ga NS with $d \approx 300$ nm. The backward scattering spectra measured for the Ga NS illuminated by *s*- and *p*-polarized light are provided for reference. e) Nonlinear response spectra measured for a Ga NS with $d \approx 240$ nm at different excitation irradiances. The backward scattering spectrum of the Ga NS is also provided. The excitation wavelength was chosen at ≈535 nm. The relationship between the slope extracted from the dependence of the luminescence intensity on the excitation irradiance and the energy of the emitted photon is shown in the inset. f) Luminescence decay measured for the Ga NS. IRF, instrumental response function.

by using a coupled charge device were presented in Figure 5c as insets.

Based on the numerical analysis given in Figure 2, more efficient white light emission from the Ga NS is expected when the Fano dip at ≈640 nm is resonantly excited by using the femtosecond laser light. We measured the luminescence spectra of Ga NS with different diameters when the excitation wavelength was fixed at 640 nm (see Figure S8, Supporting Information). It can be seen that the strongest hot-electron luminescence was achieved in the Ga NS whose Fano resonance was resonant with the excitation wavelength (i.e., $d \approx 280$ nm). In addition, we also measured the excitation spectrum for the Ga NS, as shown in Figure 5d, where the backward scattering spectra of the Ga NS illuminated by *s*- and *p*-polarized light are also provided for reference. It can be seen that the strongest white light emission is achieved at the Fano dip (i.e., the scattering valley).

In Figure 5e, we present the luminescence spectra measured for a Ga with $d \approx 240$ nm at different irradiances. The excitation wavelength was chosen at ≈535 nm. In this case, efficient hot-electron luminescence could be achieved at very low excitation irradiances and enhanced luminescence was observed at the MD resonnace (≈700 nm). If we raised the excitation irradiance, however, the Ga NS was easily damaged probably due to the heat accumulation at the contacting point between the Ga NS and the Ag film, which leads to the explosion of the liquid Ga NS. Therefore, we could only characterize the dependence of the luminescence intensity on the excitation irradiance in the low excitation irradiance regime, which exhibits a slope close to 1.0, as shown in the inset of Figure 5e. We also measured the luminescence lifetime for the Ga NS placed on the Ag film, as shown in Figure 5e. The lifetime derived from the luminescence decay was found to be shorter than 10 ps, which is beyond the time resolution of our instrument. Since the hot luminescence in this case is dominated by the intraband transition of hot electrons, it indicates the fast relaxation of hot electrons through emitting photons in the conduction band.[43,55]

4. Conclusions

In summary, we have successfully fabricated Ga NSs with a core-shell structure and investigated the linear and nonlinear optical responses of such Ga NSs placed a glass slide and a thin Ag film. It was demonstrated that the surface plasmon resonance of Ga NSs can be tuned from the visible light to near-infrared spectral region by varying the diameter of Ga NSs. It was found that a Fano resonance can be created by exploiting the coherent interaction between the MD mode and the GP mode induced by a thin Ag film. The existence of the Fano resonance was verified by the significantly enhanced electric field inside the Ga NSs. In contrast to the weak nonlinear optical responses of Ga NSs placed on a glass slide, a significantly enhanced broadband luminescence was observed for the Ga NSs placed on the thin Ag film when the mirror-image-induced MD resonance or the Fano dip was resonantly excited by using femtosecond laser pulses. Based on the spectral analysis of the slope extracted from the dependence of the luminescence intensity on the excitation irradiance, the broadband luminescence was identified as hot-electron intraband luminescence whose lifetime was found to be shorter than 10 ps. Apparently, the fabricated Ga NSs offer an ideal platform on which the linear and nonlinear optical properties of single Ga NSs, the manipulation of directional radiation, and the effects of phase transition on the optical properties can be systematically investigated. The efficient white light emission from Ga NSs makes them a promising candidate for nanoscale incandescent light sources which may be applied in nanospectrocopy, bioimaging, and active photonic devices.[35,36]

Supporting Information

Supporting Information is available from the Wiley Online Library or from the author.

Acknowledgements

J.X. and J.C. contributed equally to this work. S. L. thanks the financial support from the National Key Research and Development Program of China (No. 2016YFA0201002). S. L. and S. T. acknowledge the financial support from the National Nature and Science Foundation of China (Grant Nos. 11674110 and 11874020), the Natural Science Foundation of Guangdong Province, China (Grant No. 2016A030308010), and the Science and Technology Planning Project of Guangdong Province, China (Grant No. 2015B090927006). J. X. thanks Innovation Project of Graduate School of South China Normal University (Grant No. 2017LKXM022).

Conflict of Interest

The authors declare no conflict of interest.

Keywords

Fano resonance, femtosecond laser ablation, gallium nanospheres, hot electron luminescence, liquid metal, magetic dipole resonance

Received: August 17, 2018
Revised: December 22, 2018
Published online:

[1] P. Albella, B. Garcia-Cueto, F. Gonzalez, F. Moreno, P. C. Wu, T.-H. Kim, A. Brown, Y. Yang, H. O. Everitt, G. Videen, *Nano Lett.* **2011**, *11*, 3531.
[2] M. W. Knight, T. Coenen, Y. Yang, B. J. M. Brenny, M. Losurdo, A. S. Brown, H. O. Everitt, A. Polman, *ACS Nano* **2015**, *9*, 2049.
[3] P. C. Wu, C. G. Khoury, T.-H. Kim, Y. Yang, M. Losurdo, G. V. Bianco, T. Vo-Dinh, A. S. Brown, H. O. Everitt, *J. Am. Chem. Soc.* **2009**, *131*, 12032.
[4] Y. Yang, J. M. Callahan, T.-H. Kim, A. S. Brown, H. O. Everitt, *Nano Lett.* **2013**, *13*, 2837.
[5] J. M. Sanz, D. Ortiz, R. Alcaraz de la Osa, J. M. Saiz, F. Gonzalez, A. S. Brown, M. Losurdo, H. O. Everitt, F. Moreno, *J. Phys. Chem. C* **2013**, *117*, 19606.
[6] P. C. Wu, M. Losurdo, T.-H. Kim, M. Giangregorio, G. Bruno, H. O. Everitt, A. S. Brown, *Langmuir* **2009**, *25*, 924.
[7] C. Yi, T.-H. Kim, W. Jiao, Y. Yang, A. Lazarides, K. Hingerl, G. Bruno, A. Brown, M. Losurdo, *Small* **2012**, *8*, 2721.
[8] P. Ghigna, G. Spinolo, G. B. Parravicini, A. Stella, A. Migliori, R. Kofman, *J. Am. Chem. Soc.* **2007**, *129*, 8026.
[9] M. Losurdo, A. Suvorova, S. Rubanov, K. Hingerl, A. S. Brown, *Nat. Mater.* **2016**, *15*, 995.
[10] B. F. Soares, F. Jonsson, N. I. Zheludev, *Phys. Rev. Lett.* **2007**, *98*, 153905.
[11] A. M. Watson, X. Zhang, R. A. de la Osa, J. M. Sanz, F. Gonzlez, F. Moreno, G. Finkelstein, J. Liu, H. O. Everitt, *Nano Lett.* **2015**, *15*, 1095.
[12] J. M. McMahon, G. C. Schatz, S. K. Gray, *Phys. Chem. Chem. Phys.* **2013**, *15*, 5415.
[13] S. Kim, J.-M. Kim, J.-E. Park, J.-M. Nam, *Adv. Mater.* **2018**, *30*, 1704528.
[14] J. J. Mock, M. Barbic, D. R. Smith, D. A. Schultz, S. Schultz, *J. Chem. Phys.* **2002**, *116*, 6755.
[15] Y. Yang, N. Akozbek, T.-H. Kim, J. Marcos Sanz, F. Moreno, M. Losurdo, A. S. Brown, H. O. Everitt, *ACS Photonics* **2014**, *1*, 582.
[16] S. Ramadurgam, T.-G. Lin, C. Yang, *Nano Lett.* **2014**, *14*, 4517.
[17] H.-W. Liu, F.-C. Lin, S.-W. Lin, J.-Y. Wu, B.-T. Chou, K.-J. Lai, S.-D. Lin, J.-S. Huang, *ACS Nano* **2015**, *9*, 3875.
[18] M. W. Knight, N. S. King, L. Liu, H. O. Everitt, P. Nordlander, N. J. Halas, *ACS Nano* **2014**, *8*, 834.
[19] S. Ayas, A. E. Topal, A. Cupallari, H. Guner, G. Bakan, A. Dana, *ACS Photonics* **2014**, *1*, 1313.
[20] Y. Gutierrez, D. Ortiz, J. M. Sanz, J. M. Saiz, F. Gonzalez, H. O. Everitt, F. Moreno, *Opt. Express* **2016**, *24*, 20621.
[21] A. Di Cicco, *Phys. Rev. Lett.* **1998**, *81*, 2942.
[22] G. B. Parravicini, A. Stella, P. Ghigna, G. Spinolo, A. Migliori, F. d'Acapito, R. Kofman, *Appl. Phys. Lett.* **2006**, *89*.
[23] M. Yarema, M. Woerle, M. D. Rossell, R. Erni, R. Caputo, L. Protesescu, K. V. Kravchyk, D. N. Dirin, K. Lienau, F. von Rohr, A. Schilling, M. Nachtegaal, M. V. Kovalenko, *J. Am. Chem. Soc.* **2014**, *136*, 12422.
[24] P. J. Bennett, S. Dhanjal, P. Petropoulos, D. J. Richardson, N. I. Zheludev, V. I. Emelyanov, *Appl. Phys. Lett.* **1998**, *73*, 1787.
[25] A. V. Krasavin, K. F. MacDonald, A. S. Schwanecke, N. I. Zheludev, *Appl. Phys. Lett.* **2006**, *89*, 031118.
[26] K. F. MacDonald, V. A. Fedotov, S. Pochon, K. J. Ross, G. C. Stevens, N. I. Zheludev, W. S. Brocklesby, V. I. Emel'yanov, *Appl. Phys. Lett.* **2002**, *80*, 1643.
[27] Y. Yu, Q. Wang, L. Yi, J. Liu, *Adv. Eng. Mater.* **2014**, *16*, 255.
[28] A. B. Evlyukhin, S. M. Novikov, U. Zywietz, R. L. Eriksen, C. Reinhardt, S. I. Bozhevolnyi, B. N. Chichkov, *Nano Lett.* **2012**, *12*, 3749.
[29] A. I. Kuznetsov, A. E. Miroshnichenko, Y. H. Fu, J. Zhang, B. Luk'yanchuk, *Sci. Rep.* **2012**, *2*, 492.
[30] J. Xiang, S. Jiang, J. Chen, J. Li, Q. Dai, C. Zhang, Y. Xu, S. Tie, S. Lan, *Nano Lett.* **2017**, *17*, 4853.

[31] C.-Y. Zhang, Y. Xu, J. Liu, J.-T. Li, J. Xiang, H. Li, J.-X. Li, Q.-F. Dai, S. Lan, A. E. Miroshnichenko, *Nat. Commun.* **2018**, *9*, 2964.
[32] J. Xiang, J. Li, Z. Zhou, S. Jiang, J. Chen, Q. Dai, S. L. Tie, S. Lan, X. Wang, *Laser Photonics Rev.* **2018**, *12*, 1800032.
[33] Z. Qian, Z. Ji, Z. Fuli, D. Lippens, *Mater. Today* **2009**, *12*, 60.
[34] R. Alaee, R. Filter, D. Lehr, F. Lederer, C. Rockstuhl, *Opt. Lett.* **2015**, *40*, 2645.
[35] S. V. Makarov, I. S. Sinev, V. A. Milichko, F. E. Komissarenko, D. A. Zuev, E. V. Ushakova, I. S. Mukhin, Y. F. Yu, A. I. Kuznetsov, P. A. Belov, I. V. Iorsh, A. N. Poddubny, A. K. Samusev, Y. S. Kivshar, *Nano Lett.* **2018**, *18*, 535.
[36] F. Lu, M. Jin, M. A. Belkin, *Nat. Photonics* **2014**, *8*, 307.
[37] G. Liu, H. Deng, G. Li, L. Chen, Q. Dai, S. Lan, S. Tie, *Plasmonics* **2014**, *9*, 1471.
[38] J.-D. Chen, J. Xiang, S. Jiang, Q.-F. Dai, S.-L. Tie, S. Lan, *Nanoscale* **2018**, *10*, 9153.
[39] I. Sinev, I. Iorsh, A. Bogdanov, D. Permyakov, F. Komissarenko, I. Mukhin, A. Samusev, V. Valuckas, A. I. Kuznetsov, B. S. Luk'yanchuk, A. E. Miroshnichenko, Y. S. Kivshar, *Laser Photonics Rev.* **2016**, *10*, 799.
[40] B. Luk'yanchuk, N. I. Zheludev, S. A. Maier, N. J. Halas, P. Nordlander, H. Giessen, C. T. Chong, *Nat. Mater.* **2010**, *9*, 707.
[41] A. E. Miroshnichenko, S. Flach, Y. S. Kivshar, *Rev. Mod. Phys.* **2010**, *82*, 2257.
[42] Y. Yang, W. Wang, A. Boulesbaa, I. I. Kravchenko, D. P. Briggs, A. Puretzky, D. Geohegan, J. Valentine, *Nano Lett.* **2015**, *15*, 7388.
[43] E. D. Palik, *Handbook of Optical Constants of Solids*, Academic Press, San Diego, CA, USA **1998**.
[44] E. Xifre-Perez, L. Shi, U. Tuzer, R. Fenollosa, F. Ramiro-Manzano, R. Quidant, F. Meseguer, *ACS Nano* **2013**, *7*, 664.
[45] J. J. Mock, R. T. Hill, A. Degiron, S. Zauscher, A. Chilkoti, D. R. Smith, *Nano Lett.* **2008**, *8*, 2245.
[46] J. Mertens, M.-E. Kleemann, R. Chikkaraddy, P. Narang, J. J. Baumberg, *Nano Lett.* **2017**, *17*, 2568.
[47] L. Chen, G. C. Li, G. Y. Liu, Q. F. Dai, S. Lan, S. L. Tie, H. D. Deng, *J. Phys. Chem. C* **2013**, *117*, 20146.
[48] S. Viarbitskaya, A. Teulle, R. Marty, J. Sharma, C. Girard, A. Arbouet, E. Dujardin, *Nat. Mater.* **2013**, *12*, 426.
[49] D. Y. Lei, A. I. Fernandez-Dominguez, Y. Sonnefraud, K. Appavoo, R. F. Haglund Jr, J. B. Pendry, S. A. Maier, *ACS Nano* **2012**, *6*, 1380.
[50] P. Saeta, J.-K. Wang, Y. Siegal, N. Bloembergen, E. Mazur, *Phys. Rev. Lett.* **1991**, *67*, 1023.
[51] K. Sokolowski-Tinten, J. Bialkowski, M. Boing, A. Cavalleri, and D. von der Linde, *Phys. Rev. B* **1998**, *58*, R11805(R).
[52] S. W. Chan, R. Barille, J. M. Nunzi, K. H. Tam, Y. H. Leung, W. K. Chan, A. B. Djurisic, *Appl. Phy. B* **2006**, *84*, 351.
[53] X-F. Li, C-Y. Zhang, H. Li, Q-F. Dai, S. Lan, and S-L. Tie, *Opt. Express* **2014**, *22*, 28086.
[54] T. Haug, P. Klemm, S. Bange, J. M. Lupton, *Phys. Rev. Lett.* **2015**, *115*, 067403.
[55] L. Roloff, P, Klemm, I. Gronwald, R. Huber, J. M. Lupton, S. Bange, *Nano Lett.* **2017**, *17*, 7914.